

Nanoscale

Accepted Manuscript



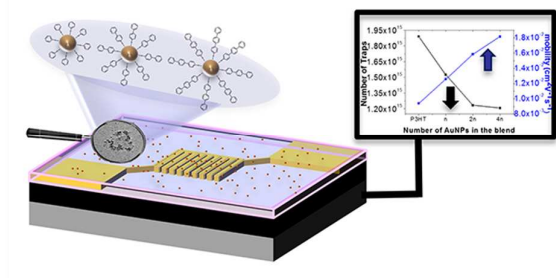
This is an *Accepted Manuscript*, which has been through the Royal Society of Chemistry peer review process and has been accepted for publication.

Accepted Manuscripts are published online shortly after acceptance, before technical editing, formatting and proof reading. Using this free service, authors can make their results available to the community, in citable form, before we publish the edited article. We will replace this *Accepted Manuscript* with the edited and formatted *Advance Article* as soon as it is available.

You can find more information about *Accepted Manuscripts* in the [Information for Authors](#).

Please note that technical editing may introduce minor changes to the text and/or graphics, which may alter content. The journal's standard [Terms & Conditions](#) and the [Ethical guidelines](#) still apply. In no event shall the Royal Society of Chemistry be held responsible for any errors or omissions in this *Accepted Manuscript* or any consequences arising from the use of any information it contains.

Table of content



We correlate the effect of size and coating of Au nanoparticles blended with P3HT on the electronic properties of the multicomponent OTFT.

Cite this: DOI: 10.1039/c0xx00000x

www.rsc.org/nanoscale

COMMUNICATION

The role of size and coating in Au nanoparticles incorporated into bi-component polymeric thin-film transistors

Thomas Mosciatti^a, Emanuele Orgiu^a, Corinna Raimondo^{a,b} and Paolo Samorì^{a,*}

Received (in XXX, XXX) Xth XXXXXXXXXX 20XX, Accepted Xth XXXXXXXXXX 20XX

DOI: 10.1039/b000000x

We describe the effect of blending poly(3-hexylthiophene) (P3HT) with Au nanoparticles (AuNPs) on the performance of organic thin-film transistors. To this end we have used AuNPs of two different sizes coated with chemisorbed SAMs of oligophenylthiols possessing increasing lengths. The electrical characteristics of the hybrid materials revealed changes in field-effect mobility depending primarily on the AuNPs size, as a result of the variable energy level of the coated metallic nanocluster and by the degree of modification of P3HT crystalline structure.

Solution-processed organic thin-film transistors (OTFTs) have garnered great attention in the last decade because they hold a huge potential as key components for large-area electronics and logic circuits.¹ Nowadays, one among the greatest challenges in such a field of research relies on the increase of the structural and functional complexity of the devices by tailoring and exploiting multicomponent, hybrid films and more generally sophisticated nanocomposites², paving the way towards multifunctional devices³. Among various organic and polymeric semiconductors, poly(3-hexylthiophene) (P3HT) is a reference component because of its easy processability in numerous solvents and large field-effect mobility in thin film⁴. Organic/inorganic hybrid materials are gaining much attention because of the possibility of varying the properties of different individual components enables the optimization of the characteristics of the overall material. Metallic nanoclusters, like gold nanoparticles (AuNPs), are space-confined objects holding unique properties determined by their nanoscale size, and by their stabilizing coating layer.⁵ However, the effect on charge transport of different sized AuNPs exposing various coating layers has never been analyzed in-depth. It is known that a transition from semiconductor to insulator occurs in AuNPs with a diameter below 1.5 nm⁶. While a bulk metallic material exhibits a continuous spectrum of states, when the very same material possesses a finite size, like a nanoparticle, the states are rather discrete. This stems from the proportionality between the density-of-states (DOS) and the number of atoms in the ensemble, leading to the formation of a band gap even in metal aggregates⁷. While bulk gold exhibits metallic behaviour, with the decreasing size of gold aggregates the DOS smoothly scales up to the formation of a band gap between energy levels (Kubo gap)⁸. The coating layer of AuNPs can consist of chemisorbed Self-Assembled Monolayers (SAMs)

of a specific molecule that imparts additional functions including a specific surface energy⁹, optoelectronic properties¹⁰ and capacity to penetrate cell-membranes¹¹. These features can be optimized by achieving control over the packing of the molecules forming SAMs on the NPs. When NPs are integrated in a device they can act as charge storage sites enabling the system to operate as a memory. Thin-film transistors incorporating blends of an organic semiconductor and AuNPs as active layer have already been studied. Previous research endeavor was focused on the effect of different sizes AuNPs or decorated with different coating layers in OTFT¹² as well as floating gates¹³, memristors¹⁴ and inverters¹⁵. Among thiol-functionalized molecules capable of chemisorbing on Au nanostructures, oligophenyl-thiols (OPTs) not only exhibit interesting electronic properties¹⁶ but can also form ordered SAMs on Au surfaces¹⁷. Because of these reasons OPTs have been used to coat the planar Au electrodes of an OTFT in order to modulate the charge injection at the metal-semiconductor interface¹⁸. Although the optical properties of AuNPs were found to be modified via chemisorption of OPTs on their surface¹⁹, it is unknown how this functionalization influences their electrical characteristics.

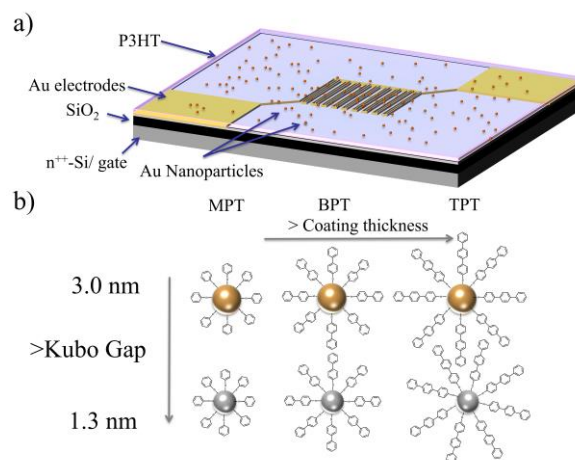


Figure 1. (a) Scheme of the bottom-contact/bottom-gate thin-film transistor using a bi-component P3HT-AuNPs blend as the active layer. (b) Schematic summary of the system: the three different oligophenylthiols used as the coating for the AuNPs (MPT, BPT, TPT) with increasing molecular length and the AuNPs encompassed in this study, semiconducting (3.0 nm) and insulating (1.3 nm), respectively

Here we show that the presence of different sized AuNPs coated with SAMs of oligophenyl-thiols (OPTs) with increasing contour length can modify structural and electrical properties of P3HT films. This includes its crystalline nature and field-effect mobility as well as bias-stress response when it acts as the active layer in bottom-contact bottom-gate TFT. We have used three linear oligophenyl-thiol derivative, i.e. (mono)phenylthiol (MPT), biphenyl-4-thiol (BPT) and 1,1',4',1''-terphenyl-4-thiol (TPT). The device scheme is portrayed in Fig. 1a while the different coating molecules are shown in Fig. 1b. We have focused our attention on AuNPs with a diameter of either 3.0 nm or 1.3 nm which, according to the Kubo rule, possess an energy gap of 6.4 meV and 80 meV, respectively, therefore being over 3 times larger or smaller than kT .⁶

Complete chemisorption of the OPTs on the two sized AuNPs has been accomplished starting from a solution of HAuCl_4 in toluene which has been reduced to metallic gold in presence of an amine followed by a ligand exchange reaction with the chosen thiolated molecule (see ESI for experimental details). The coated AuNPs have been characterized by UV-Vis absorption and TEM (see ESI). Up to six different samples types were prepared and tested in OTFTs: pristine P3HT, P3HT/AuNPs-3.0 nm coated with MPT, BPT and TPT blends, and P3HT/AuNPs-1.3 nm coated with MPT and BPT. Unfortunately 1.3 nm AuNPs coated with TPT could not be studied because their synthesis turned out to be extremely difficult due to low solubility of TPT in all the attempted solvents (toluene, tetrahydrofuran, acetone, chloroform, dichloromethane, chlorobenzene, dichlorobenzene). For the sake of comparison we also prepared 3.0 nm-AuNPs coated with a saturated SAM of octadecylamine (ODA) to get greater insight into the role of the coating layer.

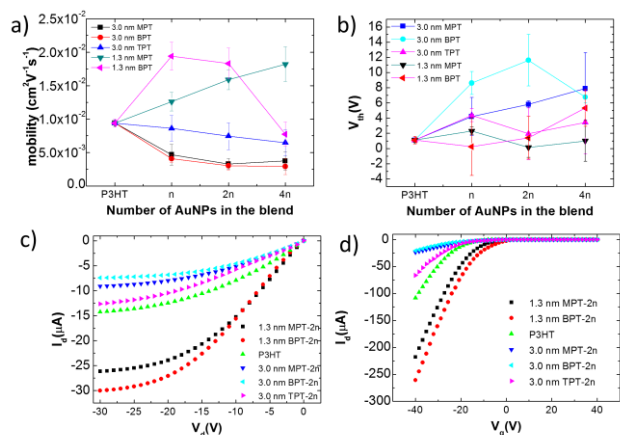


Figure 2. Comparative plots of (a) field-effect mobility vs. blend composition. (b) Threshold voltage devices for all the different blends for channel length $10 \mu\text{m}$. (c) Output and (d) transfer characteristics for OTFTs and 2n-blends with AuNPs ((c) with $V_g = -20$ V) for channel lengths of $10 \mu\text{m}$.

We have chosen to compare blends of P3HT with 1.3 nm and 3 nm AuNPs incorporating the same number of AuNPs. For this purpose $1.8 \cdot 10^{14}$ (n), $3.6 \cdot 10^{14}$ (2n), $7.2 \cdot 10^{14}$ (4n) AuNPs of the two sizes have been added to P3HT maintaining the weight-to-weight ratio of P3HT with the solvent always at 1 mg/ml. Those values of AuNPs correspond to percentages in weight of AuNPs with respect to P3HT of 5%, 10%, 20% for AuNPs-3.0 nm and 0.25%,

0.5%, 1% for AuNPs-1.3 nm. The devices have been prepared by spin coating of the blends on bottom-contact bottom-gate TFTs followed by thermal annealing at 75°C for 2 hours, as detailed in the ESI. Results on the electrical characteristics, performed in N_2 atmosphere, relied on a statistics of over 30 devices for every different combination of AuNPs size/coating type.

All devices exhibited a very good p-type behavior, responding with an almost ideal spacing between curves at different gate voltages (see ESI for details). The extracted mobilities (μ) from saturation regime are reported in Table S2 and are plotted in Fig. 2a. They reveal that the use of 3.0 nm AuNPs induces a universal three-fold decrease in mobility for n-NPs blends when compared to pristine P3HT and differently coated AuNPs exhibited a similar electrical behavior, with the field-effect mobility which decreases with the increasing quantity of AuNPs in the blend. The type of coating seems not to influence notably the mobility: MPT and BPT blends exhibit the same trend and values, whereas TPT blends show the same trend with slightly higher μ values which is likely due to the greatest tendency of this type of AuNPs to aggregate, ultimately reducing the occurrence of scattering centers within the film. Conversely, AuNPs-1.3 nm devices present an increase of mobility. Significantly, MPT blends reveal a linear enhancement in mobility up to 100% with the increasing number of AuNPs in the blend. For BPT there is a two-fold enhancement in mobility already for n-blends while for 4n-blends the μ drops down to a value slightly lower than pristine P3HT devices. OTFT devices based on P3HT blends with 1.3 nm AuNPs coated with as much as MPT 2.25% in weight (10n) revealed $\mu = (8.7 \pm 1.4) \times 10^{-3} \text{ cm}^2 \text{V}^{-1} \text{s}^{-1}$. Such a result demonstrates that with the increasing quantity of 1.3 nm sized AuNPs in the blend, after an initial increase in μ , a decrease is observed. The latter finding can be likely ascribed to inter-particle aggregation when large quantities of AuNPs in the blend material are used, as discussed in the next paragraphs. The increase in mobility in P3HT/AuNPs based OTFTs was already reported^{12b}, and a strong dependence on the concentration of AuNPs in the blend was found. However, here we demonstrate how the contribution of size and type of coating of the AuNPs are two entangled parameters. In order to provide a comparative picture of the different electrical properties of the different blends, Fig. 2c-d displays the output and transfer characteristic of 2n-blend of AuNPs compared to pure P3HT based devices. It shows a higher mobility and a maximum current reached for 1.3 nm AuNPs/P3HT active layers, both parameters decreasing in 3.0 nm AuNPs/P3HT blends.

Threshold voltage (V_{th}) have also been extracted from the transfer curves in the saturation regime. V_{th} values were larger and positive at small channel lengths for all the different blends (see ESI for details), which is a marked short-channel effect coming from the bare semiconductor as observable in the pristine P3HT values. In Fig. 2b are reported the values of V_{th} for 2n-blends with different coating and size. There is a general shift toward more positive values for P3HT/AuNPs devices, but increasing the number of AuNPs does not lead to a clear trend though they would all be comprised in the 0 - 10 V range which makes it appealing for low-power dissipation applications. It is interesting to take into account other studies on similar system for V_{th} shift in AuNPs/P3HT OTFTs showing tunable values of the

V_{th} with AuNPs concentration^{15b}. We believe that a major role is played by the coating type as evidenced by the dependence of the V_{th} on the chemisorbed SAM and the amount of coated AuNPs in the film, although a general trend on V_{th} vs. the concentration of AuNPs in P3HT is not evident. Moreover, it is worth noting the error bars associated with V_{th} that can be ascribed to the poor homogeneous dispersion of AuNPs in the blend films prepared by spin coating, indicative of locally randomly distributed NPs aggregates.

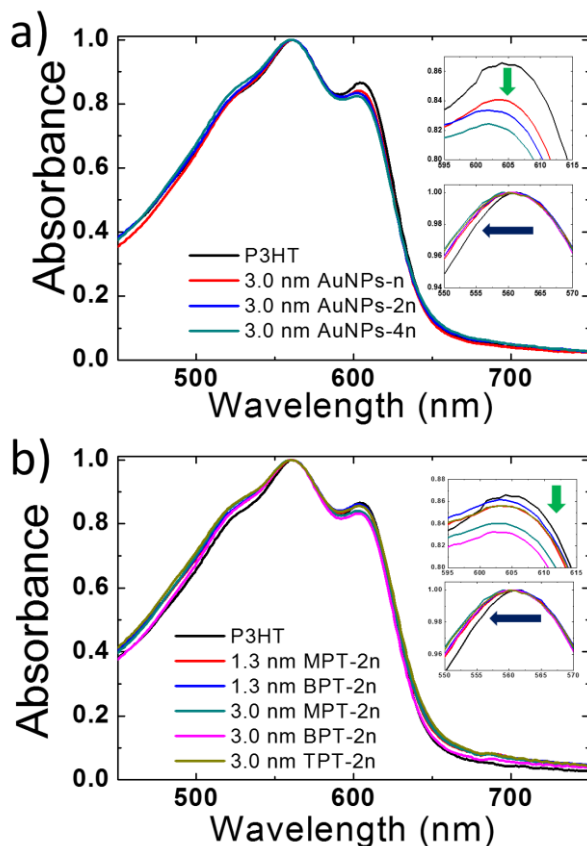


Figure 3. (a) Absorption spectra of P3HT/AuNPs-3.0 nm BPT with different load of AuNPs (n, 2n, 4n) compared to pristine P3HT. Spectra are normalized to the maximum at $\lambda=560$ nm to better show the variation of the peak related to the 0-0 transition. (b) Normalized absorption spectra of all the P3HT/AuNPs-2n blends compared to pristine P3HT.

To shine more light onto the role of the coating layer we have extended our studies to devices incorporating 3.0 nm AuNPs in a number of 4n coated with the saturated ODA monolayer. ODA is a well-known reducing agent²⁰, but is not possible to obtain AuNPs smaller than 3 nm because amines are weak ligands for AuNPs²¹. The devices exhibited a mobility of $(6.6 \pm 5.2) \times 10^{-4} \text{ cm}^2 \text{ V}^{-1} \text{ s}^{-1}$, being one order of magnitude lower when compared to pristine P3HT and 50-folds lower compared to the worst performing P3HT/AuNPs-3.0 nm 4n devices. Also it displayed a shift of V_{th} towards more negative values up to 14 V for $L = 20 \mu\text{m}$, revealing overall poor device characteristics if compared to the others blend combination. This effect can be ascribed to three factors: (i) a more modest purification which is achieved with ODA-AuNPs, because they tend to aggregate after 5 cycles of centrifugation, (ii) the electrically insulating character of the

octadecyl chain acting as an electrical barrier, and (iii) the weak physical interaction between the amino group and gold which could be perturbed by the presence of the sulfur atom of P3HT²².

To gain insight into the effect of AuNPs on the morphology of P3HT films we carried out UV-Vis measurements. The P3HT film exhibits two transitions in the UV-Vis spectral range, i.e. the 0-0 and the 0-1 transition. These transitions can be explained in the framework of the H-aggregate model²³. The 0-0 transition arises from the weak $\pi-\pi$ interaction between crystalline parts forming H-aggregates while the 0-1 is due to inter-chain states of disordered chains. The relative intensity of such bands is determined by the free exciton bandwidth (W) of aggregates which is inversely proportional to the percentage of crystalline aggregates in the film.²⁴ The value obtained for W (see ESI) is ca. 20 meV for all the different blends, which is indicative of a high percentage of crystalline aggregates within the film.²⁴ However, Fig. 3a reveals that the increase in AuNPs content is accompanied by a decrease in the relative intensity of the 0-0 peaks as well as a peak broadening, indicating a lower $\pi-\pi$ interaction between P3HT chains thus a decrease in the general order of the polymer in the film. The addition of further more AuNPs causes a larger decrease of the intensity of the 0-0 peak providing evidence for an increased disorder, the latter being responsible for the decreased mobility in the devices. Figure 3b compares the difference in absorbance for all 2n blends. AuNPs-3.0 nm TPT exhibits a lower decrease at $\lambda=602$ nm, indicating weaker perturbation of the P3HT crystalline structure when compared the other two coatings. It is worth noting that pristine AuNPs and blend P3HT/AuNPs exhibit different aggregation propensities and morphologies as monitored by TEM (Fig. S2 and S4 in the ESI). For 3.0 nm AuNPs the coating plays a major role, in fact AuNPs-3.0 nm TPT strongly aggregate while, an ordered honeycomb arrangement was found for AuNPs-3.0 nm BPT. If dispersed in P3HT (Fig. S4) the NPs are much less aggregated, with TPT coated nanoparticles presenting still some tendency to form clusters. This result can be attributed to the presence of a longer oligophenylene chain in TPT causing stronger $\pi-\pi$ interactions between TPT-TPT and TPT-P3HT. This finding is reflected in the relatively greater mobility measured in AuNPs coated TPT based devices with respect to MPT and BPT. On the other hand, 1.3 nm sized AuNPs are well dispersed on the TEM grid but in a P3HT matrix they tend to aggregate more, forming small clusters of NPs. However, a very mild decrease in the absorption 0-0 peak for 2n blends is observed, due to the smaller perturbation of the P3HT crystalline structure induced by the smaller AuNPs size.

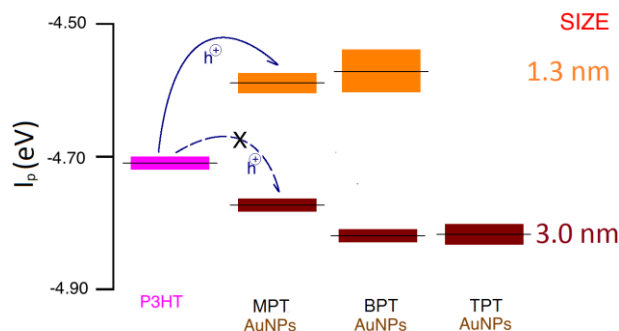


Figure 4. Ionization potential of the employed components.

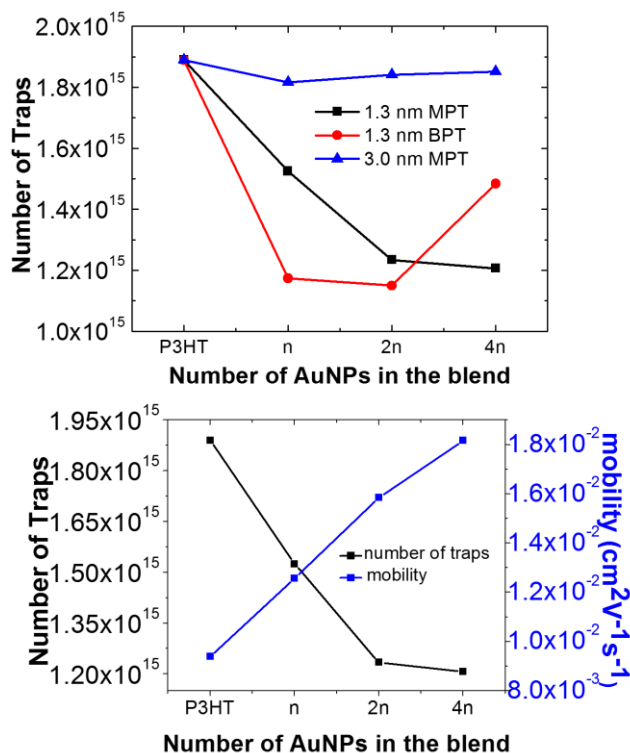


Figure 5. (a) Plot of the number of traps vs. different blends percentage of AuNPs for AuNPs-1.3 nm MPT and BPT, and AuNPs-3.0 nm MPT as a comparison. The first point is referred to P3HT. (b) Comparison of number of traps vs. mobility for AuNPs-1.3 nm MPT.

To gain a greater understanding, we have performed ambient photoelectron spectroscopy measurements to quantify the ionization potential (I_p) of bare P3HT films and AuNPs with different sizes and coatings (Fig. 4). P3HT thin film spun from solution in chlorobenzene exhibited a $I_p = 4.68$ eV, in agreement with previous reports.²⁵ AuNPs have been drop casted in 35 nm thick films on gold and then measured: 3.0 nm-AuNPs exhibit a I_p which lies about 100 meV below that of P3HT, hence out of the band gap of P3HT. This means that no favorable hole interaction is possible between P3HT and AuNPs, which can only act as a scattering centers for charges. 1.3 nm-AuNPs possess an I_p of ca. 80 meV above that of P3HT, i.e. its I_p is sitting inside the band gap of the active polymeric semiconductor. This favorable energetics will allow the 1.3 nm-AuNPs to interact with charge carriers transported in the P3HT matrix at the HOMO level. Interestingly, these results are in contrast with the Kubo gap theory for the sole NPs that predicts a bigger band gap for smaller nanoparticles, i.e. the HOMO levels of AuNPs-1.3 nm should be placed outside the band gap while should be the opposite for 3.0 nm AuNPs. However, we believe that the mismatch can arise from the effect of a different number of sulphur-gold dipoles which is directly proportional to the number of gold atoms in the two types of NPs, i.e. 1.3 nm and 3.0 nm. The less are the atoms present in a cluster the more the energetic level are affected of the sulfur-gold bond enthalpy which is more exothermic in NPs with respect to gold in flat surfaces²⁶. In our case the different contribution to the dipole from oligophenyl thiols is negligible because they possess a very similar structure, thus the energy level shift should depend mainly on the different number of gold atoms in different size NPs, being ca. 900 and 50 atoms for the

35 3.0 nm and 1.3 nm AuNPs, respectively.

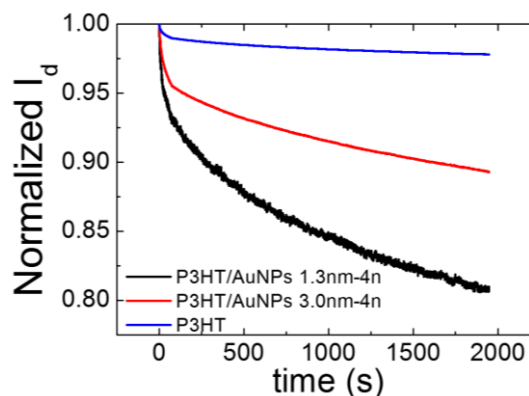


Figure 6. Normalized current with respect to the initial current vs. time for P3HT devices, and AuNPs blends (4n-BPT) of the different sizes.

To better understand the meaning and the consequences of the I_p measurements, we executed Space-Charge-Limited Current (SCLC) measurements to calculate the number of traps present in the active layers with different blends²⁷. The SCLC model is based on the analysis of three different current regimes: a first regime which follows Ohm's law, a second regime which is governed by Child's law for solids and a third one, entered once all the trap levels are filled up. In particular, a characteristic threshold voltage called trap-filled limit voltage (V_{TFL}) has to be overcome in order to enter the trap-filled regime. According to the SCLC theory, the number of electrical traps in a semiconducting material is directly proportional to the trap-filled limited voltage (V_{TFL}) and its electrical permittivity, thereby making it possible to extract the density of traps from the I-V curve, using the equation (1)²⁸

$$N_t = \frac{\epsilon V_{TFL}}{eL^2} \quad (1)$$

Where L is the inter-electrodes distance, ϵ is the dielectric permittivity of the semiconductor and e is the elementary charge. The values, obtained from those measurements with a statistic of 16 samples for each blend are plotted in Fig. 5a. The value we used for the calculation of relative electrical permittivity of P3HT is 3.3²⁹. Pristine semiconductor devices present a number of traps of the order of magnitude of 10^{15} and all AuNPs-3.0 nm blends present about the same number of traps of P3HT with no variation regarding the percentage or the coating layer. Conversely, devices incorporating 1.3 nm sized AuNPs revealed a more modest amount of traps, with values up to 25% lower respect to P3HT pristine devices. For those small NPs a higher percentage present less traps for MPT coating, while for BPT coating there is a decrease of traps at small percentage and then an increase for 4n-blends. For those two system the mobility values follow an opposite trend (as shown for AuNPs-1.3 nm MPT devices in Fig. 4b): they become bigger when adding NPs-MPT coated, while for NPs-BPT coated it decreases at 4n-blend. This mirroring behavior between mobility and number of traps confirm the fact that 1.3 nm AuNPs electronically interact with P3HT and that their presence fill traps in the P3HT electronic

structure, leading to higher mobility. On the other hand, 3.0 nm AuNPs do not affect charge transport in P3HT based OTFT.

To further address the effect of the presence of AuNPs, we have studied the behavior of transistor under a constant bias-stress voltage applied to the drain. It is well known that P3HT based OTFT show a decrease of current until a plateau is reached,³⁰ as determined by charge trapping inside deep energy states of P3HT³¹. We measured the drain current in function of time, for 10% blend of AuNPs-BPT coated devices, by applying a constant bias stress at the drain $V_d = -5$ V and a gate voltage V_g calculated from the threshold voltage of the device extracted from the saturation regime with $V_g - V_{th} = -5$ V for a time of 30 minutes. The drain current decreases in the first minutes and reaches a plateau at different time depending of the sample (see Fig. 6 with a normalized current with respect to the initial current on the Y-axis). A statistic over 8 devices with variable percentage variation revealed that pristine devices exhibit the smallest time decay, with a minor fatigue, reaching a well stable plateau. AuNPs blends displayed a larger fatigue and decay time of two orders of magnitude lower with respect to pristine P3HT. 1.3 nm-AuNPs devices do not reach the plateau after the end of the measure; they have the biggest decrease of current and bigger time decay which is indicative of a better electronic interaction with the active layer. Conversely, 3.0 nm-AuNPs devices exhibited a reduced current decay if compared to the former ones. This can be seen as an undesired presence of defects in the film which lowers the possibility for the charges to percolate. By decreasing the nanoparticle size, 1.3 nm-AuNPs electronically interact with P3HT by acting as doping agent, thereby increasing mobility of a factor up to two. However, an excess of 1.3 nm-AuNPs in the blend led to a decrease of performance. On the other hand, the effect of the coating layer is subtle but not less important. It influences very much the aggregation tendency of NPs, thus influencing the mobility and while giving subtle variation on the V_{th} .

Conclusions

We have shown that the size of AuNPs markedly affects the charge transport mechanism in OTFTs based on P3HT blended with AuNPs coated with OPTs. In particular, OPT coated AuNPs with a 1.3 nm diameter were observed to electronically interact with P3HT, increasing the OTFT device performances without significantly disrupting the crystalline nature of the P3HT film. On the other hand, bigger AuNPs, i.e. with a 3 nm diameter, were found not to interact electronically with P3HT, and just act as scattering centres for charges, while slightly altering the P3HT crystalline aggregates. AuNPs coated with different chemisorbed SAMs exhibited different behaviors, in particular determined by the different tendency of the AuNPs to aggregate, indirectly influencing the field-effect mobility. Overall, we have showed that the use of AuNPs in bi-component hybrid TFTs is a simple yet powerful method for modifying the physical and chemical properties of a polymeric semiconductor. Being based on thiol-based chemisorption, this approach combines a simple synthesis route with an easy processability and a high reproducibility. Noteworthy, the possibility of tuning different characteristics, i.e. size and coating, can lead to an enhancement of the electronic properties in OTFTs. Therefore, the use of AuNP has a double

advantage: it enables the improvement of the performance of OTFTs and the integration of multiple functions in a single device, towards smart logic solutions.

Acknowledgments

This work was financially supported by EC through the Marie-Curie ITN SUPERIOR (PITN-GA-2009-238177), the ERC project SUPRAFUNCTION (GA-257305), the Agence Nationale de la Recherche through the LabEx project Chemistry of Complex Systems (ANR-10-LABX-0026_CSC), and the International Center for Frontier Research in Chemistry (icFRC).

Notes and references

^a Nanochemistry Laboratory, ISIS – CNRS 7006, Université de Strasbourg, 8 allée Gaspard Monge, 67000 Strasbourg, France. Email – samori@unistra.fr, FAX: +33 368 85 52 32

^b Present address: Northwestern University, 2145 Sheridan Road Tech Evanston, IL, USA.

[†] Electronic Supplementary Information (ESI) available: [details of any supplementary information available should be included here]. See DOI: 10.1039/b000000x/

1. a) A. C. Arias, J. D. MacKenzie, I. McCulloch, J. Rivnay and A. Salleo, *Chem. Rev.*, 2010, **110**, 3-24; b) A. Dodabalapur, *Mater. Today*, 2006, **9**, 24-30; c) S. R. Forrest, *Nature*, 2004, **428**, 911-918; d) G. H. Gelinck, H. E. A. Huitema, E. van Veenendaal, E. Cantatore, L. Schrijnemakers, J. B. P. H. van der Putten, T. C. T. Geuns, M. Beenhakkers, J. B. Giesbers, B.-H. Huisman, E. J. Meijer, E. M. Benito, F. J. Touwslager, A. W. Marsman, B. J. E. van Rens and D. M. de Leeuw, *Nat Mater*, 2004, **3**, 106-110; e) H. Sirringhaus, *Adv. Mater.*, 2009, **21**, 3859-3873; f) E. C. P. Smits, S. G. J. Mathijssen, P. A. van Hal, S. Setayesh, T. C. T. Geuns, K. A. H. A. Mutsaers, E. Cantatore, H. J. Wondergem, O. Werzer, R. Resel, M. Kemerink, S. Kirchmeyer, A. M. Muzafarov, S. A. Ponomarenko, B. de Boer, P. W. M. Blom and D. M. de Leeuw, *Nature*, 2008, **455**, 956-959.
2. M. Caironi, T. D. Anthopoulos, Y.-Y. Noh and J. Zaumseil, *Adv. Mater.*, 2013, **25**, 4208-4209.
3. a) Y. Guo, G. Yu and Y. Liu, *Adv. Mater.*, 2010, **22**, 4427-4447; b) N. Crivillers, E. Orgiu, F. Reinders, M. Mayor and P. Samorì, *Adv. Mater.*, 2011, **23**, 1447-1452.
4. H. Sirringhaus, P. J. Brown, R. H. Friend, M. M. Nielsen, K. Bechgaard, B. M. W. Langeveld-Voss, A. J. H. Spiering, R. A. J. Janssen, E. W. Meijer, P. Herwig and D. M. de Leeuw, *Nature*, 1999, **401**, 685-688.
5. a) R. Klajn, J. F. Stoddart and B. A. Grzybowski, *Chem. Soc. Rev.*, 2010, **39**, 2203-2237; b) H. Otsuka, Y. Nagasaki and K. Kataoka, *Advanced Drug Delivery Reviews*, 2003, **55**, 403-419.
6. R. Kubo, A. Kawabata and S. Kobayashi, *Annual Review of Materials Science*, 1984, **14**, 49-66.
7. R. Kubo, *J. Phys. Soc. Jpn.*, **17**, 975.
8. E. Roduner, *Chem. Soc. Rev.*, 2006, **35**, 583-592.
9. A. S. Karakoti, S. Das, S. Thevuthasan and S. Seal, *Angew. Chem. Int. Ed.*, 2011, **50**, 1980-1994.
10. F. Seker, P. R. L. Malenfant, M. Larsen, A. Alizadeh, K. Conway, A. M. Kulkarni, G. Goddard and R. Garaas, *Adv. Mater.*, 2005, **17**, 1941-1945.
11. A. Verma, O. Uzun, Y. Hu, Y. Hu, H.-S. Han, N. Watson, S. Chen, D. J. Irvine and F. Stellacci, *Nat Mater*, 2008, **7**, 588-595.
12. a) M.-C. Wong, S.-C. Yeh, L.-K. Chiu, Y.-H. Chen, J.-R. Ho and R. C.-C. Tsiang, *J. Nanosci. Nanotechnol.*, 2012, **12**, 2292-2299; b) S.-T. Han, Y. Zhou, Q.-D. Yang, C.-S. Lee and V. A. L. Roy, *Part. Part. Syst. Char.*, 2013, **30**, 599-605; c) C. Raimondo, N. Crivillers, F. Reinders, F. Sander, M. Mayor and P. Samorì, *Proc. Natl. Acad. Sci. U.S.A.*, 2012, **109**, 12375-12380.
13. C.-W. Tseng, D.-C. Huang and Y.-T. Tao, *ACS Appl. Mater. Interfaces*, 2013, **5**, 9528-9536.

14. a) F. Alibart, S. Pleutin, O. Bichler, C. Gamrat, T. Serrano-Gotarredona, B. Linares-Barranco and D. Vuillaume, *Adv. Funct. Mater.*, 2012, **22**, 609-616; b) C. Novembre, D. Guerin, K. Lmimouni, C. Gamrat and D. Vuillaume, *Appl. Phys. Lett.*, 2008, **92**, 103314; c) A. Prakash, J. Ouyang, J.-L. Lin and Y. Yang, *J. Appl. Phys.*, 2006, **100**, 054309-054309-054305.
15. a) Y. Zhou, S.-T. Han, L.-B. Huang, J. Huang, Y. Yan, L. Zhou and V. A. L. Roy, *Nanotechnology*, 2013, **24**, 205202; b) S.-T. Han, Y. Zhou, Z.-X. Xu and V. A. L. Roy, *Appl. Phys. Lett.*, 2012, **101**, 033306-033305.
16. a) A. M. Masillamani, N. Crivillers, E. Orgiu, J. Rotzler, D. Bossert, R. Thippeswamy, M. Zharnikov, M. Mayor and P. Samorì, *Chem. Eur. J.*, 2012, **18**, 10335-10347; b) M. Bürkle, J. K. Viljas, D. Vonlanthen, A. Mishchenko, G. Schön, M. Mayor, T. Wandlowski and F. Pauly, *Phys. Rev. B*, 2012, **85**, 075417.
17. W. Azzam, B. I. Wehner, R. A. Fischer, A. Terfort and C. Wöll, *Langmuir*, 2002, **18**, 7766-7769.
18. E. Orgiu, N. Crivillers, J. Rotzler, M. Mayor and P. Samorì, *J. Mater. Chem.*, 2010, **20**, 10798-10800.
19. M. Busby, C. Chiorboli and F. Scandola, *J. Phys. Chem. B*, 2006, **110**, 6020-6026.
20. D. V. Leff, L. Brandt and J. R. Heath, *Langmuir*, 1996, **12**, 4723-4730.
21. D. S. Sidhaye and B. L. V. Prasad, *New J. Chem.*, 2011, **35**, 755-763.
22. L. Zhai and R. D. McCullough, *J. Mater. Chem.*, 2004, **14**, 141-143.
23. F. C. Spano, *J. Chem. Phys.*, 2005, **122**, 234701.
24. J. Clark, J.-F. Chang, F. C. Spano, R. H. Friend and C. Silva, *Appl. Phys. Lett.*, 2009, **94**, 163306-163311.
25. E. Orgiu, N. Crivillers, M. Herder, L. Grubert, M. Pätzelt, J. Frisch, E. Pavlica, D. T. Duong, G. Bratina, A. Salleo, N. Koch, S. Hecht and P. Samorì, *Nat Chem*, 2012, **4**, 675-679.
26. J. R. Reimers, Y. Wang, B. O. Cankurtaran and M. J. Ford, *J. Am. Chem. Soc.*, 2010, **132**, 8378-8384.
27. M. A. Lampert and P. Mark, *Current Injection in Solid*, Academic Press, 1970.
28. M. A. Lampert, A. Rose and R. W. Smith, *J. Phys. Chem. Solids*, 1959, **8**, 464-466.
29. K. Müller, M. Richter, S. Philip, M. Kunst and D. Schmeißer, *BioNanoSci.*, 2012, **2**, 42-51.
30. M. Estrada, I. Mejía, A. Cerdeira, J. Pallares, L. F. Marsal and B. Iñiguez, *Solid-State Electron.*, 2009, **53**, 1063-1066.
31. Y. R. Liu, R. Liao, P. T. Lai and R. H. Yao, *Device and Materials Reliability, IEEE Transactions on*, 2012, **12**, 58-62.